FNT/T-98/11
CERN-TH/98-356

Light Pair Correction to Bhabha Scattering at Small Angle

G.Montagna [a] M.Moretti [b,c] O.Nicrosini [a]
A.Pallavicini [a] F.Piccinini [a]

[a] *Dipartimento di Fisica Nucleare e Teorica - Università di Pavia and INFN - Sezione di Pavia, via A. Bassi 6, Pavia, Italy*

[b] *Theory Division, CERN, CH-1211 Geneva 23, Switzerland*

[c] *Dipartimento di Fisica - Università di Ferrara and INFN - Sezione di Ferrara, Ferrara, Italy*

Abstract

This work deals with the computation of electron pair correction to small angle Bhabha scattering, in order to contribute to the improvement of luminometry precision at LEP/SLC below 0.1% theoretical accuracy.

The exact QED four-fermion matrix element for $e^+e^- \to e^+e^-e^+e^-$, including all diagrams and mass terms, is computed and different Feynman graph topologies are studied to quantify the error of approximate calculations present in the literature.

Several numerical results, obtained by a Monte Carlo program with full matrix element, initial-state radiation via collinear structure functions, and realistic event selections, are shown and critically compared with the existing ones.

The present calculation, together with recent progress in the sector of $O(\alpha^2)$ purely photonic corrections, contributes to achieve a total theoretical error in luminometry at the 0.05% level, close to the current experimental precision and important in view of the final analysis of the electroweak precision data.

Keywords: electron-positron collision, small angle Bhabha scattering, theoretical error, light pairs, Monte Carlo
PACS: 02.70.Lq,12.15.Lk,13.40.Ks,13.85.Hd

1 Introduction

The high-precision determination of the machine luminosity at LEP/SLC is an essential ingredient of the success of precision tests of the electroweak interactions on top of the Z resonance [1].

As well known, the Bhabha scattering process at small angle (of the order of a few degrees) is the reference reaction used for luminosity monitoring at LEP/SLC, owing to its large cross section (dominated by t-channel photon exchange) and its substantial independence of purely electroweak effects. Experimental efforts in the development of efficient, dedicated luminometry detectors, as well as precision calculations of the small-angle Bhabha (hereafter SABH) scattering cross section both contribute to achieve a measurement of the "Z factories" luminosity with a total relative error at the 0.1% level [1, 2, 3]. On the experimental side, the present total uncertainty is smaller than 0.1% [2], close to the 0.05 level [4]. As far as the theory contribution to the luminosity measurement is concerned, the estimate of the theoretical errors, used by the LEP collaborations, is summarized in table 1 [3] for centre of mass energies around and above the Z resonance.

Table 1: Theoretical error in SABH scattering according to ref. [3] at typical LEP1 and LEP2 energies.

Type of correction/error	LEP1 (%)	LEP2 (%)
missing photonic $O(\alpha^2 L)$	0.100	0.200
missing photonic $O(\alpha^3 L^3)$	0.015	0.030
vacuum polarization	0.040	0.100
light pairs	0.030	0.050
Z-exchange	0.015	0.000
total	0.110	0.250

Some comments on table 1 are in order. The components of the theoretical error refer to the SABH scattering cross section, for any typical event selection of LEP experiments, as computed by the program `BHLUMI v4.03` [5]. The largely dominating source of theoretical error is due to the missing part of $O(\alpha^2 L)$ subleading photonic corrections, where $L = \ln(-t/m^2)$ is the collinear logarithm in t-channel scattering. Also the contribution of the

missing part of the leading $O(\alpha^3 L^3)$ corrections is of photonic nature. The vacuum polarization entry is the effect of the uncertainty in the hadronic contribution to the running of $\alpha_{\rm QED}$, when considering the parameterization and relative error estimate of ref. [6]. The next contribution is the uncertainty introduced by the corrections due to the production of light pairs, chiefly e^+e^- ones. The last entry refers to the uncertainty associated to the treatment of the γ-Z interference. More details about the strategy adopted in order to estimate the various sources of theoretical error can be found in ref. [3].

After the analysis of ref. [3], important theoretical developments took place. Additional work in the sector of two-loop photonic corrections [7, 8] led to the conclusion that the perturbative contribution due to the uncontrolled part of $O(\alpha^2 L)$ corrections does not exceed the 0.03% level. This conclusion has been very recently reinforced by the detailed analysis of ref. [4]. Furthermore, new determinations [9] of $\alpha_{\rm QED}$ lower the error on hadronic contribution to vacuum polarization in s-channel processes at $\sqrt{s} = M_Z$. This might affect SABH scattering too, although no dedicated analysis for the low-angle regime exists yet.

As a consequence of this progress, it is relevant to reduce the uncertainty associated to the light pair contribution. At present, the calculations available in the literature and used to estimate the light pair uncertainty as given in table 1 concern a Monte Carlo (hereafter MC) computation based on an approximate t-channel matrix element [10] and to an analytical approach with fixed event selections [11]. Previous leading logarithmic evaluations of the dominant light pair contribution to SABH can be found in ref. [12].

In order to improve the existing situation and contribute to the lowering of the light pair error, in the present paper a MC calculation is drawn with the exact $e^+e^- \to e^+e^-e^+e^-$ matrix element and taking into account realistic event selections. The analysis is chiefly presented at LEP1/SLC energies ($\sqrt{s} = 92$ GeV), but numerical results are shown at LEP2 energies ($\sqrt{s} = 176$ GeV) too. The impact of the present calculation in the reduction of the theoretical error for LEP/SLC luminosity measurement is also discussed.

The outline of the paper is as follows. The details concerning the treatment of phase space are described in section 2, while in section 3 the selection criteria considered in the present study are reviewed. Section 4 is devoted to describe the calculation. The last sections contain a discussion of numerical results, including comparison with existing analytical calculations (section 5) and approximate MC results (section 6), as well as study of the effect

of initial-state radiation (hereafter ISR) (section 7). The conclusions and possible developments are given in section 8.

2 Phase Space Generation

Pair corrections to Bhabha scattering lead to a four-body kinematics and to an 8-dimensional phase space. Expansion in few body processes can greatly simplify the phase space parameterization. The choice between different equivalent expansions should be suggested by the relevant dynamics.

At high energies and small momentum transfer, which is of interest for luminosity measurements at LEP, the leading contribution to cross section is given by bremsstrahlung Feynman graphs sketched in figure 1, i.e. by t-channel photon exchange dynamics. Indeed, since the relevant dynamics is dominated by pure QED processes, weak effects, such as Z-exchange or multiperipheral graphs mediated by at least one Z boson, will be neglected in the following. Further the present study deals mainly with electron pair production, because it is known [3, 11] that heavier particles give a much smaller contribution.

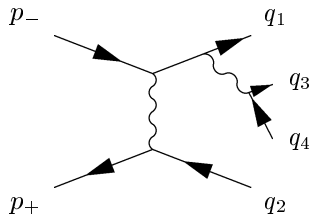

Figure 1: One of the sixteen bremsstrahlung graphs representing the leading t-channel dynamics.

Let us define the photon momentum $k \equiv q_3 + q_4$ and its energy by $\omega \equiv k_0$. The core of bremsstrahlung contribution is given by the soft pair approximation, i.e. the limit $|t| \gg \omega, |\vec{k}|$. In this regime the emitted pair is almost collinear to the photon k. Thus the phase space configurations in which q_3 and q_4 are back-to-back are highly suppressed by t-channel dynamics.

However, the selection criteria for kinematic events, used by the LEP collaborations and reviewed in section 3, scan also the hard region. When

bremsstrahlung processes get smaller, the next to leading Feynman graph topology is represented by multiperipheral dynamics shown in figure 2. Notice that this contribution is relevant also for $\gamma\gamma$ physics, being described in its bulk by the Weizsäcker-Williams approximation [13] for which the internal photons become quasi-real.

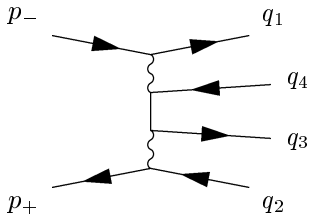

Figure 2: One of the eight Feynman diagrams for multiperipheral dynamics.

Bremsstrahlung and multiperipheral graphs do not complete all the Feynman graph topologies. Other two classes of diagrams can be drawn, namely the annihilation and conversion ones, which are shown in figure 3. Their contribution is less important at high energies and small momentum transfer. Thus in this paper phase space parameterization and importance sampling does not deal with these configurations.

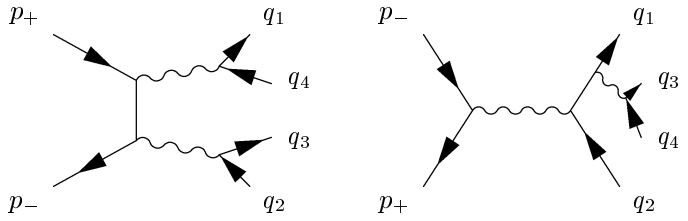

Figure 3: Two of the twelve Feynman diagrams representing conversion and annihilation dynamics, respectively.

The two following subsections show how the kinematics is treated according to the previous considerations about the dynamics.

2.1 Phase Space for Bremsstrahlung Events

2.1.1 Phase Space Parameterization

Let us consider the four-body phase space for two incoming particles of momentum p_- and p_+, and four outgoing particles of momentum $q_1 \dots q_4$. Let us define $P \equiv p_- + p_+$.

$$d^8R_4(P; q_1, q_2, q_3, q_4) \equiv \prod_{i=1}^{4} \frac{d^3q_i}{2E_i} \delta^{(4)}(P - \sum_{i=1}^{4} q_i) \tag{1}$$

The four-body kinematics can be split into the product of simpler processes. t-channel dynamics suggests to think of the event as formed by a fermionic current interacting with a particle which radiates a pair. Thus let us deal with the event as a three body plus a two body kinematics. The following decomposition can be introduced

$$d^8R_4(P; q_1, q_2, q_3, q_4) = d^5R_3(P; q_1, q_2, q_{34}) d^2R_2(q_{34}; q_3, q_4) ds_{34} \tag{2}$$

where s_{34} is the squared mass of $q_{34} \equiv q_3 + q_4$.

The three body kinematics can be expressed in terms of invariants. Let us define $s_{ij\dots} \equiv (q_i + q_j + \dots)^2$ and $t_{\pm j\dots} \equiv (p_\pm - q_j - \dots)^2$. A straightforward calculation leads to

$$d^5R_3(P; q_1, q_2, q_{34}) = \frac{1}{32\lambda^{1/2}(s, m^2, m^2)\sqrt{-\Delta_4}} \, ds_{12} dt_{-34} ds_{134} dt_{+2} d\varphi \tag{3}$$

where $d\varphi$ integration is over the beam direction, λ is the Källen function and Δ_4 is the fourth order symmetric Gram determinant.

The two body kinematics gets the simpler form

$$d^2R_2(q_{34}; q_3, q_4) = \frac{\lambda^{1/2}(s_{34}, m^2, m^2)}{8s_{34}} d^2\Omega_3^* \tag{4}$$

where Ω_3^* is the solid angle of q_3 in the frame in which $\vec{q}_{34} = 0$.

2.1.2 Physical Region

The physical region depends on the choice of the order of integration for the phase space variables. Let us consider the following choice (read up-down then left-right)

ds_{34}	dR_3	dR_2
s_{34}	s_{12}	$\cos\theta_3^*$
	t_{-34}	φ_3^*
	s_{134}	
	t_{+2}	

With this ordering the limits for the phase space variables are

$$
\begin{aligned}
s_{34} &\in [4m^2, (s^{1/2} - 2m)^2] \\
s_{12} &\in [4m^2, (s^{1/2} - s_{34}^{1/2})^2] \\
t_{-34} &\in \left[m^2 + s_{34} - \Big(\frac{s + s_{34} - s_{12}}{2} + \sqrt{\frac{1}{4} - \frac{m^2}{s}} \lambda^{1/2}(s, s_{34}, s_{12}) \Big), \right. \\
&\quad \left. , m^2 + s_{34} - \Big(\frac{s + s_{34} - s_{12}}{2} - \sqrt{\frac{1}{4} - \frac{m^2}{s}} \lambda^{1/2}(s, s_{34}, s_{12}) \Big) \right] \qquad (5) \\
s_{134} &\in \left[m^2 + s_{34} - \Big(\frac{s_{12} + s_{34} - s}{2} + \sqrt{\frac{1}{4} - \frac{m^2}{s_{12}}} \lambda^{1/2}(s, s_{34}, s_{12}) \Big), \right. \\
&\quad \left. , m^2 + s_{34} - \Big(\frac{s_{12} + s_{34} - s}{2} - \sqrt{\frac{1}{4} - \frac{m^2}{s_{12}}} \lambda^{1/2}(s, s_{34}, s_{12}) \Big) \right] \\
t_{+2} &\in \{ t_{+2} : \Delta_4 \leq 0 \}
\end{aligned}
$$

These limits are exact, thus the phase space generation has efficiency equal to one if no selection criterion is set on.

2.1.3 Importance Sampling

The soft pair limit provides a relatively simple analytical approximation for the t-channel contribution to the cross section. This expression can be reached either from direct calculation or from analytic results available in the literature [14]. The resulting integral gives a guideline to sample the full cross section formula.

According to the choice for the phase space variables ordering, the weights w follow

$$
\begin{aligned}
w(s_{34}) &= \frac{1}{s_{34}} \\
w(s_{12}) &= \begin{cases} 1/(s+s_{34}-s_{12}) \propto (1/E_{34}) & , s_{12} \geq s'_{12} \\ 1 & , s_{12} \leq s'_{12} \end{cases} \\
w(t_{-34}) &= \frac{1}{m^2 - t_{-34}} \\
w(s_{134}) &= \frac{1}{s_{134} - m^2} \\
w(t_{+2}) &= \begin{cases} 1 & , t_{+2} \leq t'_{+2} \\ 1/(t^2_{+2}) & , t'_{+2} \leq t_{+2} \leq t''_{+2} \\ 1/(-t_{+2}) & , t_{+2} \geq t''_{+2} \end{cases}
\end{aligned}
\tag{6}
$$

where $w(s_{34})$ and $w(s_{12})$ deal with the infrared pole, $w(t_{-34})$ and $w(s_{134})$ with the collinear pole, and $w(t_{+2})$ with the coulomb pole. The boundaries s'_{12}, t'_{+2} and t''_{+2} should be set according to the selection criteria.

2.2 Phase Space for Multiperipheral Events

Multiperipheral events require true four-body kinematics, since no natural expansion of the phase space can fit the dynamics, because of the three propagators between the ingoing particles. Thus a description based on energies and angles can be preferred to an invariant picture.

2.2.1 Phase Space Parameterization

Let us integrate out q_4 and put $E_i \equiv q_{i,0}$

$$
d^8 R_4(P; q_1, q_2, q_3, q_4) = \delta(E - \sum_{i=1}^{4} E_i) \frac{d^3 q_1}{2E_1} \frac{d^3 q_2}{2E_2} \frac{d^3 q_3}{2E_3} \frac{1}{2E_4} \tag{7}
$$

where E_1, E_2 and E_3 are given by mass shell relations and E_4 by energy-momentum conservation.

Let us consider the decay $k \to q_3, q_4$ where $k \equiv q_3 + q_4$, $\omega \equiv k_0$, and $s_{34} \equiv k^2$. The three momentum $|\vec{q}_3|$ and the cosine of the polar angle θ_3, with respect to a fixed direction $\hat{\vec{u}}_z$, are needed as phase space variables. Let us write $\vec{k}$ as $\vec{k} = k_z \hat{\vec{u}}_z + k_x \hat{\vec{u}}_x$ the third axis being defined as $\hat{\vec{u}}_y = \hat{\vec{u}}_z \times \hat{\vec{u}}_x$. Energy conservation implies that

$$\begin{aligned}\omega^2 + E_3^2 - 2\omega E_3 &= m^2 + |\vec{q}_3|^2 + |\vec{k}|^2 - 2k_z|\vec{q}_3|\cos\theta_3 + \\ &\quad -2k_x|\vec{q}_3|\sin\theta_3\sin\varphi_3 \end{aligned} \tag{8}$$

namely

$$\sin\varphi_3 = \frac{1}{2k_x|\vec{q}_3|\sin\theta_3}(2\omega E_3 - s_{34} - 2k_z|\vec{q}_3|\cos\theta_3) \tag{9}$$

The Jacobian is easily obtained as

$$J^{-1} = \frac{k_x|\vec{q}_3|\sin\theta_3\cos\varphi_3}{E_4} \tag{10}$$

This leads to the following phase space parameterization

$$\begin{aligned} d^8R_4(P;q_1,q_2,q_3,q_4) &= \frac{1}{16k_xE_1E_2E_3|\vec{q}_3|\sin\theta_3\cos\varphi_3}\times \\ &\quad d|\vec{q}_1|d^2\Omega_1 d|\vec{q}_2|d^2\Omega_2 d|\vec{q}_3|d\cos\theta_3 \end{aligned} \tag{11}$$

where $k_x = (\vec{P} - \vec{q}_1 - \vec{q}_2)\cdot\hat{\vec{u}}_x$, $E_i = \sqrt{m^2 + |\vec{q}_i|}$, and $d^2\Omega_i \equiv d\cos\theta_i d\varphi_i$.

2.2.2 Physical Region

The physical region is given by

$$|2k_x|\vec{q}_3|\sin\theta_3| \geq |2\omega E_3 - \omega^2 + s_{34} - 2k_z|\vec{q}_3|\cos\theta_3| \tag{12}$$

which means ($\sin\theta_3 \geq 0$)

$$\begin{aligned} 2(k_x|\vec{q}_3|\sin\theta_3 - \omega E_3 + k_z|\vec{q}_3|\cos\theta_3) &\geq -\omega^2 + s_{34} \\ 2(k_x|\vec{q}_3|\sin\theta_3 + \omega E_3 - k_z|\vec{q}_3|\cos\theta_3) &\geq \omega^2 - s_{34} \end{aligned} \tag{13}$$

By taking into account that $|\vec{q}_3| \leq \sqrt{|\vec{q}_3|^2 + m^2} \leq |\vec{q}_3| + m$ it follows that the range of interest is certainly contained into the domain

$$\begin{aligned} 2(k_x\sin\theta_3 - \omega + k_z\cos\theta_3)|\vec{q}_3| &\geq -\omega^2 + s_{34} \\ 2(k_x\sin\theta_3 + \omega - k_z\cos\theta_3)|\vec{q}_3| &\geq \omega^2 - s_{34} - 2\omega m \end{aligned} \tag{14}$$

which leads to

$$\frac{\omega^2 - s_{34}}{2(k_x \sin\theta_3 + \omega - k_z \cos\theta_3)} \leq |\vec{q}_3| \leq \frac{\omega^2 - s_{34}}{2(\omega - k_x \sin\theta_3 - k_z \cos\theta_3)} \qquad (15)$$

if $\omega - k_x \sin\theta_3 - k_z \cos\theta_3 > 0$
The maximum and minimum of $|\vec{q}_3|$ are achieved for $\vec{q}_3$ collinear to $\vec{k}$ in the forward and backward direction, respectively.

2.2.3 Importance Sampling

The Weizsäcker-Williams equivalent photon approximation [13] provides a useful guideline to deal with the contribution of multiperipheral diagrams. The resulting integral shows how to sample the full cross section formula by introducing the weights

$$w(\cos\theta_1) = \frac{1}{-t_{-1}(\cos\theta_1)} \quad , \quad w(\cos\theta_2) = \frac{1}{-t_{+2}(\cos\theta_2)} \qquad (16)$$

where $w(\cos\theta_1)$ and $w(\cos\theta_2)$ mimic the most singular behaviour of the Weizsäcker-Williams spectrum. t_{-1} and t_{+2} are equal to $(p_- - q_1)^2$ and $(p_+ - q_2)^2$, respectively, as previously defined. Further a flat importance sampling can be made on $\cos\theta_3$ to match the selection criteria better.

3 Selection Criteria

Two types of selection criteria are considered: `BARE1` and `CALO2`. They were defined by the "Event Generators for Bhabha Scattering" working group during the CERN Workshop "Physics at LEP2" (1994/1995), see ref. [3] for more details.

These algorithms are tailored to Bhabha scattering with photon emission. Thus they must be modified to fit with pair emission, chiefly to deal with identical particles and with fermion clusters.

3.1 A Simple Setup: `BARE1`

This non-calorimetric criterion selects events with one or more particles per calo. If more than one particle hits a calo it chooses the most energetic hit, the reference particle. Thus for each kinematic event two particles are labelled as the emitted pair and the other two as the beam particles.

Table 2: Angular acceptances in degrees for BARE1 and CALO2 algorithms.

	BARE1		CALO2	
	Left Calo	Right Calo	Left Calo	Right Calo
WW	$2.70 \to 7.00$	$2.70 \to 7.00$	$2.97 \to 6.73$	$2.97 \to 6.73$
NN	$3.30 \to 6.30$	$3.30 \to 6.30$	$3.49 \to 6.11$	$3.49 \to 6.11$
NW	$3.30 \to 6.30$	$2.70 \to 7.00$	$3.49 \to 6.11$	$2.97 \to 6.73$

Then the beam particles are selected by their energies and angles. The angular cut can be made with the same acceptance for the two caloes (wide-wide and narrow-narrow), or with different acceptances (narrow-wide).

$$\begin{array}{lcl} 3.3^\circ \leq \theta \leq 6.3^\circ & - & \text{narrow acceptance} \\ 2.7^\circ \leq \theta \leq 7.0^\circ & - & \text{wide acceptance} \end{array} \tag{17}$$

Angular acceptances are summarized in table 2. Further the energy cut is imposed by considering the adimensional variable z as usually done in the literature [10]

$$z \equiv 1 - \frac{E_1 E_2}{E_{\text{beam}}^2} \leq z_{\max} \tag{18}$$

It is worth noticing that small values of z means soft pair emission, while large values allows for hard pair radiation.

3.2 A Calorimetric Setup: CALO2

This selection criterion looks for any particle in two caloes, the former is along the ingoing electron direction, the latter is along the ingoing positron direction. Then it scans the detected particles in each calo to pick up the most energetic one, the reference particle.

It defines a cluster for each reference particle. The shape of the cluster is a square in the (θ, φ) plane of the corresponding calo, its size is of $3\Delta\theta/16 \times 3\pi/16$ radiants, where $\Delta\theta$ is the calo polar width. The cluster center is pinned to the reference particle. The cluster energy is the sum of the energies of the particles in the cluster itself.

The last step of the algorithm is to reject the events according to an angular and an energy cut, where angles are referred to the cluster center

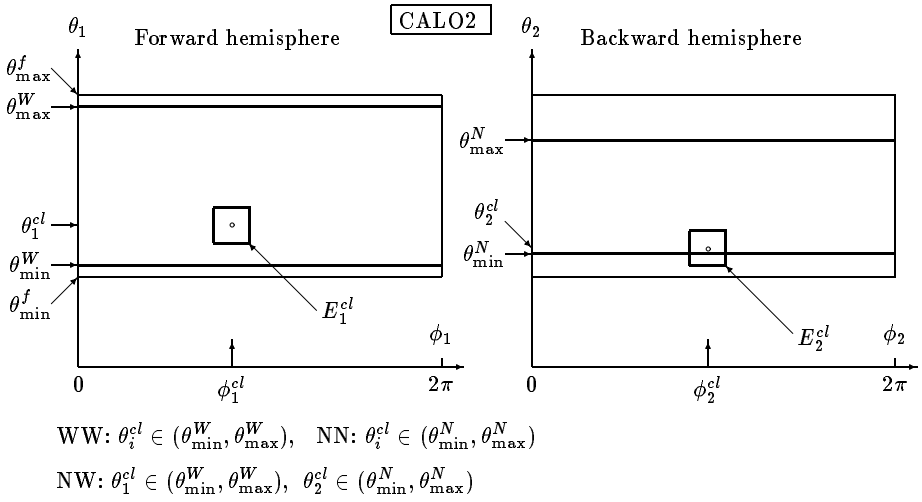

Figure 4: Geometry and acceptances of CALO2 calorimetric setup. From ref. [3].

and energies to the cluster energy. Each polar width must be reduced to an effective acceptance, as shown in figure 4, to prevent the cluster square to exceed the calo size, i.e. should the reference particle be out of the effective acceptance but within the calo total width, yet the event is rejected.

The angular cut can be made with the same polar width for the two caloes, defining a wide-wide and a narrow-narrow acceptance, or with different widths for the two caloes, defining a narrow-wide acceptance

$$\begin{array}{lcl} 3.3^\circ \leq \theta \leq 6.3^\circ & - & \text{width for narrow acceptance} \\ 2.7^\circ \leq \theta \leq 7.0^\circ & - & \text{width for wide acceptance} \end{array} \tag{19}$$

Angular acceptances are summarized in table 2. Further the energy cut is imposed by considering the adimensional variable z as given by eq. (18).

4 Dynamics Calculation

Generators including the full set, or part, of the QED diagrams for $e^+e^- \to e^+e^-l^+l^-$ ($l = e, \mu, \tau$) was already described in ref. [16] and they are used for analysis and simulation of $\gamma\gamma$ collision processes at LEP and other e^+e^- colliders.

In the present paper the MC program PAIRS, written in FORTRAN, was built to compute the $e^+e^- \to e^+e^-e^+e^-$ process. It implements the importance samplings and the selection criteria sketched previously, and computes the exact matrix element, including all mass terms, by using the ALPHA algorithm and the resulting code [15], that is conceived for the automatic computation of tree-level multi-particle production amplitudes without any need of Feynman graphs expansion.

Without entering the details of the algorithm ALPHA it is worth noticing, for the aim of the present study, that the predictions of this automatic algorithm have been already compared with diagrammatic results for processes with four fermions in the final state [17] showing an excellent agreement, and also successfully used to obtain original results for other reactions [18].

The main features of the program PAIRS can be summarized as follows. The code computes the phase space integral by means of an importance sampling both for bremsstrahlung and multiperipheral graphs. Since the contribution of the other topologies is small, as discussed in section 2, there is no need of a specific strategy to reduce the associated variance.

The integration is performed in two steps. In the former the matrix element is sampled by using the bremsstrahlung weights, see section 2.1.3. Then a rejection algorithm selects the events belonging to the phase space region Ω_B which is preferred by the bremsstrahlung dynamics. In the latter the same calculation scheme is performed in terms of the multiperipheral weights, see section 2.2.3, and of a rejection algorithm selecting the remaining phase space region Ω_M, which is preferred by the multiperipheral dynamics. The treatment of the interference between the two dynamics is addressed below.

After phase space generation the program deals with identical particles and other symmetries of the amplitude. Feynman expansion in pure QED shows sixteen bremsstrahlung graphs, eight with initial-state emission and eight with final-state emission of a fermion pair. These two families can be sampled at the same time leading only to eight different weights, which can be obtained, fixed one of them, by repeated application of identical fermion exchange symmetry (ID symmetry) or of CP symmetry. Let us note that under these symmetries the squared amplitude does not change. There are also eight multiperipheral graphs, four with an amplitude value and four, obtained twisting the kernel fermion lines (TW symmetry), with a different value. The two multiperipheral squared amplitudes are left invariant by the ID symmetry.

The symmetries of the integrand allow us to cast the cross section formula in a simpler form, because the phase space jacobians and the selection criterion characteristic functions share these symmetries too.

An example can clarify the importance of the integrand symmetries. Let us consider a function $f(x,y)$, symmetric under the change $x \to y$, which is integrated over the unit square in the (x,y) plane. In order to draw the calculation some weights are introduced, for definiteness say $\omega_1 \equiv 1/(x+a)$ $(a>0)$ is a suited weight because of some pathology in $x=-a$, but, since $f(x,y)$ is symmetric under coordinate exchange, it must also exhibit the same pathology in $y=-a$. Thus the weight $\omega_2 \equiv 1/(y+a)$ must be introduced too. The integration by using importance sampling follows.

$$\begin{aligned}
&\int_0^1 dx \int_0^1 dy\, f(x,y) = \int_0^1 dx \int_0^1 dy \left(\frac{\omega_1 f(x,y)}{\omega_1+\omega_2} + \frac{\omega_2 f(x,y)}{\omega_1+\omega_2} \right) = \\
= &\int_0^1 \frac{dx}{x+a} \int_0^1 dy\, \frac{(x+a)(y+a)}{x+y+2a} f(x,y) + \\
&+ \int_0^1 dx \int_0^1 \frac{dy}{y+a}\, \frac{(x+a)(y+a)}{x+y+2a} f(x,y) = \\
= &\; 2 \int_0^1 dx \int_{\ln a}^{\ln(a+1)} d\mu\, \frac{(x+a)(y+a)}{x+y+2a} f(x,y)
\end{aligned} \tag{20}$$

In the last step coordinate exchange symmetry both of $f(x,y)$ and integration region was used, and the integration measure changed in order to include the weight by putting $d\mu \equiv dy/(y+a)$.

Hence the illustrated two channel sampling can be collapsed into a single integration, because the integrand and the integration region share the same symmetries. The same strategy can also be adopted for the more complex integral involved in the present calculation.

Let us name by x the phase space coordinates, by $d^8R_4(x)$ the phase space volume element defined by eq. (1), by N the cross section normalization, by $\chi(x)$ the characteristic function of the selection criterion, by $p_i^B(x)$ the eight sets of weights for the bremsstrahlung amplitude and by $p_i^M(x)$ and $p_i^M(x_{\rm TW})$ the four weights for each of the multiperipheral amplitudes. These quantities share the symmetry properties

$$\begin{array}{lcll}
d^8R_4(x_i) & = & d^8R_4(x) & \forall i \in \{ID, CP, TW\} \\
\chi(x_i) & = & \chi(x) & \forall i \in \{ID, CP, TW\} \\
|M(x_i)|^2 & = & |M(x)|^2 & \forall i \in \{ID, CP\} \\
p_i^{B,M}(x_j) & = & p_j^{B,M}(x_i) & \forall i,j \in \{ID, CP, TW\}
\end{array} \tag{21}$$

where x_i is a phase space point obtained from x applying a suited symmetry among ID, CP, and TW.
In terms of these quantities the cross section integral becomes

$$\begin{aligned}\sigma &= 8N \int_{\Omega^B} \frac{d^8 R_4(x) p^B(x) \chi(x)}{\sum_{i\in\{ID,CP\}} p_i^B(x)} \sum_{\text{spin}} |M(x)|^2 + \\ & \quad 4N \int_{\Omega^M} \frac{d^8 R_4(x) p^M(x) \chi(x)}{\sum_{i\in\{ID,TW\}} p_i^M(x)} \sum_{\text{spin}} \left(|M(x)|^2 + |M(x_{TW})|^2 \right) \end{aligned} \quad (22)$$

This technique is very useful because it permits to treat twenty-four channels as they were three.

The above division of phase space leaves some problem in the bremsstrahlung region because of the interferences between t-channel and multiperipheral dynamics. Thus it is useful to add an extra flat channel to the first integral of eq. (22). The flat channel deals also with a multiperipheral contribution so it must be sampled further by the $p_i^M(x)$ weights. Hence the cross section integral is

$$\begin{aligned}\sigma &= 8N \int_{\Omega^B} \frac{d^8 R_4(x) p^B(x) \chi(x)}{\sum_{i\in\{ID,CP\}} p_i^B(x) + \eta} \sum_{\text{spin}} |M(x)|^2 + \\ & \quad 8N\eta \int_{\Omega^B} \frac{d^8 R_4(x) p^M(x) \chi(x)}{p^M(x) \left(\sum_{i\in\{ID,CP\}} p_i^B(x) + \eta \right)} \sum_{\text{spin}} |M(x)|^2 + \\ & \quad 4N \int_{\Omega^M} \frac{d^8 R_4(x) p^M(x) \chi(x)}{\sum_{i\in\{ID,TW\}} p_i^M(x)} \sum_{\text{spin}} \left(|M(x)|^2 + |M(x_{TW})|^2 \right) \end{aligned} \quad (23)$$

where η is a suitable weight for the flat channel.

The matrix element is computed by functionally integrating the QED tree level effective lagrangian with the iterative algorithm `ALPHA`, which gives directly the total amplitude $M(x)$.

After the cross section is computed for the real contribution, also the virtual correction [19] corresponding to pair emission is added. The resulting pair contribution is then normalized against the tree level Bhabha scattering cross section. The final result can be corrected for initial-state radiation via collinear structure functions too [20].

5 Comparison between MC Results and Analytical Calculations

Before the numerical results being worked out, the MC program is now tested against analytical results already present in the literature [11]. Such calculations are available for fixed selection criteria, among which one resembling `BARE1` algorithm.

A direct comparison, which could be affected by some bias because of analytical approximations and possibly small differences in the selection criterion, is shown in figure 5 and table 3 for the absolute value of the pair correction. Solid line represents analytical computation of ref. [11], while markers show the results of the present MC calculation. The error bars are within the markers. Entry values are in pb, sum up both real and virtual part, and are computed for the `BARE1` setup with symmetric angular acceptance $1.375^\circ \leq \theta \leq 3.323^\circ$ at $\sqrt{s} = 92.3$ GeV.

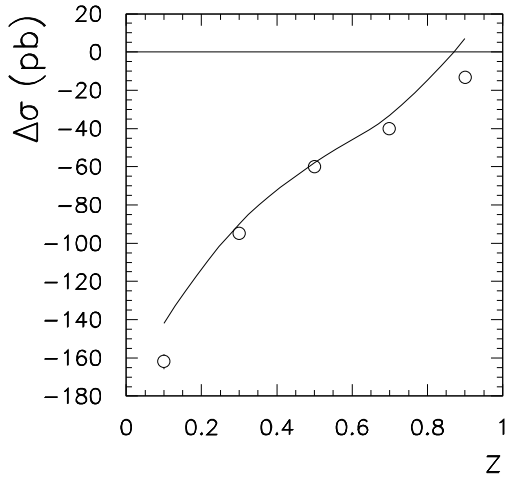

Figure 5: Comparison between MC integration of the exact matrix element (markers) and analytical computation of ref. [11] (solid line) as a function of the energy cut z, as given by eq.(18). Entry values sum up real plus virtual cross sections, and are computed for `BARE1` setup with symmetric acceptance $1.375^\circ \leq \theta \leq 3.323^\circ$ at $\sqrt{s} = 92.3$ GeV.

Table 3 shows that the relative difference between numerical and analytical results is within 15% for the experimentally relevant values of z

Table 3: Comparison between present numerical results and analytical ones of ref. [11] with the same settings of figure 5. Entry values are in pb. In this setup Bhabha tree level cross section is $\sigma_0 = 175426(14)$ pb. The error on σ_0 is due to numerical integration.

	$z = 0.1$	$z = 0.3$	$z = 0.5$	$z = 0.7$	$z = 0.9$
Present MC	-162 ± 4	-95 ± 1	-60 ± 2	-40 ± 3	-13 ± 3
Analytical	-142	-90	-58	-33	$+7$

($0.3 \leq z \leq 0.7$), thus providing a rather satisfactory test of the MC program. Further checks were performed with the results of ref. [11] for `CALO2` event selection leading to a similar behaviour.

6 Comparison between Exact Matrix Element and t-Channel Approximation

Numerical computations already present in the literature are limited to bremsstrahlung graphs without fermion exchange and up-down interference [10]. Let us define such an approach as t-channel approximation. This approximation, together with the analytical work of ref. [11], is an essential ingredient to estimate the theoretical error associated with light pair correction to SABH scattering.

As far as the MC calculation of ref. [10] is concerned, the uncertainty is the sum of a physical error, due to the incomplete matrix element calculation, and a technical error, due to algorithm stability and finite CPU time. In ref. [10] the physical error associated to the matrix element for real pair production is estimated to be 30%. Once the virtual correction is added, the cancellation against the real part can increase the magnitude of the error. In ref. [10] summing up all the sources of physical and technical uncertainty leads to a conservative estimate of the light pair correction of $-1.3 \times 10^{-4} \pm 2 \times 10^{-4}$ for narrow-wide CALO2 acceptance at $z = 0.5$ at LEP1/SLC energies. Thus the comparison of t-channel approximation with the full matrix element computation can size the magnitude of the physical error, and therefore lowers the theoretical error.

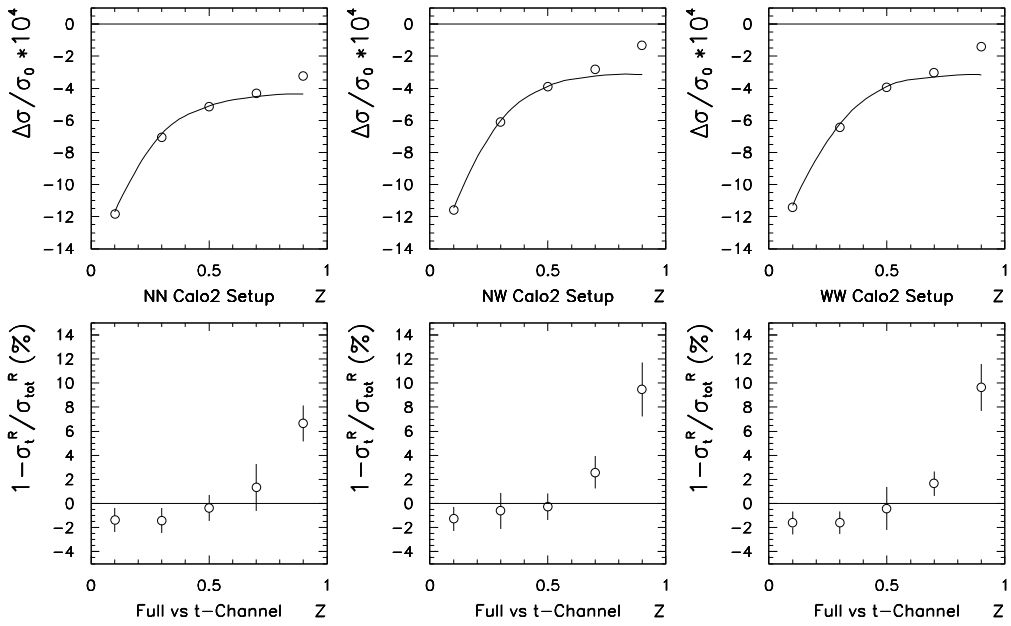

Figure 6: In the upper row: exact matrix element (markers) vs t-channel approximation (solid line) as a function of the energy cut z, as given by eq.(18). Entry values sum up real plus virtual cross sections, and are computed by varying the angular acceptances of CALO2 setup at LEP1/SLC energies. In the lower row: relative difference between the exact matrix element and t-channel approximation still as a function of the energy cut. Entry values refer only to the real pair production cross section.

In order to remove any spurious effect in the comparison between such calculations and the present one, the amplitude has been directly calculated in t-channel approximation by using the ALPHA algorithm[1] and comparing that amplitude with the full amplitude within the same selection criteria. Further the same virtual correction [19] for both the cross sections is implemented.

[1]Since the ALPHA approach does not make use of Feynman graph expansion, this is not entirely straightforward. The goal is achieved as follows: the input lagrangian is modified by introducing two distinct photons γ_1 and γ_2. The electron couples to both photons, whereas the muon and the tau lepton couples to γ_1 and γ_2, respectively. Within this modified lagrangian $m_\tau = m_\mu = m_e$ is assigned and the process $e^+\mu^- \to e^+\mu^-\tau^+\tau^-$ is studied. It is immediately seen that this reproduces the t-channel approximation.

The results are shown in figure 6 for CALO2 setup and different angular acceptances at LEP1/SLC energies. In the first row the solid line represents the t-channel approximation, while the markers the results of the present full calculation. Entries are normalized to Bhabha tree level cross section (σ_0) and sum up both real and virtual part. In the second row the markers represent the relative difference between the real part of the t-channel approximation (σ_t^{R}) and the real part of the full calculation ($\sigma_{\mathrm{tot}}^{\mathrm{R}}$).

The comparison shows appreciable differences only for $z \geq 0.7$, without much sensitivity to angular acceptance variation. By increasing z greater than 0.7, the relative difference between the real part of the cross sections can grow up to 15%.

Table 4: Comparison between exact and t-channel approximation numerical results for narrow-wide CALO2 setup, see figure 7. Entry values are in pb except for the last column. In this setup Bhabha tree level cross section is $\sigma_0 = 21939(1)$ pb. The error on σ_0 is due to numerical integration.

	Full Dynamics	t-Channel	Abs.Diff.	Rel.Diff. (%)
$z = 0.1$	-25.36 ± 0.01	-25.48 ± 0.02	0.12 ± 0.02	0.48 ± 0.08
$z = 0.3$	-12.85 ± 0.05	-13.34 ± 0.02	0.49 ± 0.05	3.67 ± 0.38
$z = 0.5$	-7.14 ± 0.05	-8.43 ± 0.02	1.29 ± 0.05	15.30 ± 0.63
$z = 0.7$	-4.98 ± 0.12	-7.06 ± 0.06	2.08 ± 0.14	29.46 ± 2.23
$z = 0.9$	-1.75 ± 0.17	-6.90 ± 0.07	5.15 ± 0.19	74.64 ± 3.51

A more refined computation is shown in figure 7, allowing a higher statistics, to get an improved accuracy in order to establish a better evaluation of the physical error. The result is shown in figure 7 and table 4 for CALO2 narrow-wide setup. The solid line represents t-channel approximation, while the markers the full calculation. The error bars are within the markers. Entry values are in pb, and sum up both real and virtual part. Table 4 shows the numerical values for the two calculations and the absolute and relative difference. Entry values are in pb.

The relative difference between the t-channel approximation and the full calculation listed in table 4 shows that the physical error, introduced by using the t-channel approximation, is within 30% for the relevant values of z. In the soft region (small z values) the relative difference gets smaller

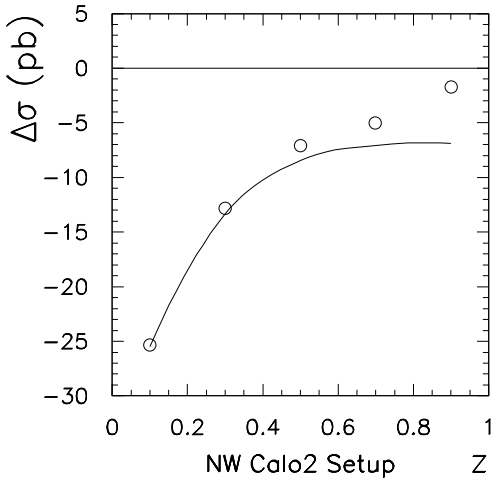

Figure 7: Results of a refined computation of the exact matrix element (markers) vs t-channel approximation (solid line) as a function of the energy cut z, as given by eq.(18). Entry values sum up real plus virtual cross sections, and are computed for narrow-wide `CALO2` setup.

since the bremsstrahlung diagrams are the largely dominating contribution at this regime. On the other hand, in the hard region (large z values) the multiperipheral diagrams become more and more relevant, worsening the agreement with the t-channel approximation.

Some tests performed at LEP2 energies show the physical error behaviour given in table 5. The difference between the exact calculation and the t-channel approximation is within 10% for the experimentally relevant z values.

The previous results refer to the `CALO2` calorimetric setup explained in section 3, where the calo acceptances are set according to ref. [10]. Yet some tests were drawn also with different angular acceptances to match the recent angular standard of LEP luminometers, as previously considered in refs. [3, 4]. The new ranges are $(1.50, 3.20)$ degrees for the wide acceptance and $(1.62, 2.84)$ degrees for the narrow acceptance at LEP1/SLC energies. The results are shown in table 6 confirming the same behaviour previously obtained.

It must be emphasized that now a MC program, that includes all the QED Feynman diagrams for $e^+e^- \to e^+e^-l^+l^-$ $(l = e, \mu, \tau)$, is available to calculate pair production corrections. Hence the physical error for electron real

Table 5: Comparison between exact and t-channel approximation numerical results for narrow-wide CALO2 setup at LEP2 energies. Entry values are in pb except for the last column. In this setup Bhabha tree level cross section is $\sigma_0 = 6087.0(3)$ pb. The error on σ_0 is due to numerical integration.

	Full Dynamics	t-Channel	Abs.Diff.	Rel.Diff. (%)
$z = 0.3$	-4.47 ± 0.01	-4.27 ± 0.01	-0.20 ± 0.02	-4.61 ± 0.24
$z = 0.5$	-2.91 ± 0.01	-2.68 ± 0.01	-0.23 ± 0.02	-8.70 ± 0.62
$z = 0.7$	-2.43 ± 0.01	-2.28 ± 0.01	-0.15 ± 0.02	-6.62 ± 0.64

Table 6: Comparison between exact and t-channel approximation numerical results for narrow-wide CALO2 setup at LEP1/SLC energies with a different choice for the angular acceptances: wide $(1.50^\circ, 3.20^\circ)$, narrow $(1.62^\circ, 2.84^\circ)$. Entry values are in pb except for the last column. In this setup Bhabha tree level cross section is $\sigma_0 = 87203(4)$ pb. The error on σ_0 is due to numerical integration.

	Full Dynamics	t-Channel	Abs.Diff.	Rel.Diff. (%)
$z = 0.3$	-41.01 ± 0.30	-43.62 ± 0.20	2.61 ± 0.36	5.99 ± 0.85
$z = 0.5$	-23.91 ± 0.42	-28.91 ± 0.25	5.31 ± 0.49	18.36 ± 1.84
$z = 0.7$	-16.99 ± 0.69	-24.99 ± 0.25	8.00 ± 0.74	32.02 ± 3.27

pair production can be reduced well below the 30% quoted in the literature. Further it is worth noticing that muon pair production was checked to be one order of magnitude smaller than the electron one.

7 Initial-State Radiation

Corrections by ISR can be evaluated by the aid of collinear QED structure functions in the non-singlet approximation [20]. Numerical computations for the previously discussed t-channel approximation are known in the literature [10]. Moreover, corrections of the order of $O(\alpha^3 L^3)$, as due to single bremsstrahlung to pair production, was analytically calculated in ref. [11].

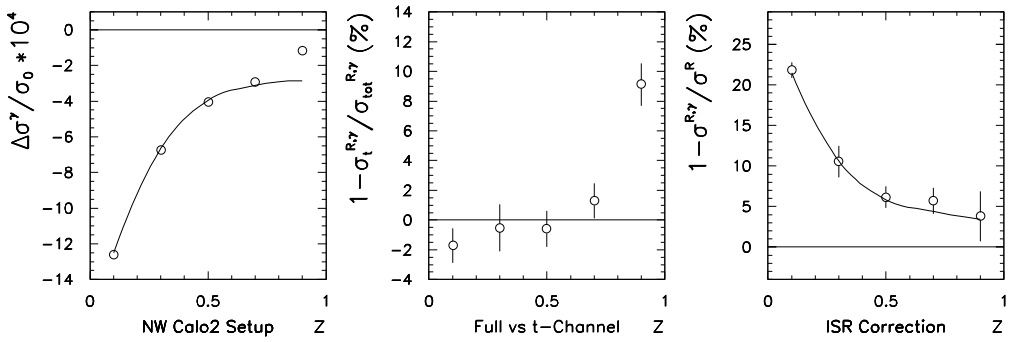

Figure 8: First picture: exact matrix element (markers) vs t-channel approximation (solid line) as a function of the energy cut z, as given by eq.(18), in the presence of ISR. Entry values sum up real plus virtual cross sections, and are computed for narrow-wide angular acceptances of CALO2 setup at LEP1/SLC energies. Second picture: relative difference between the exact matrix element and t-channel approximation till as a function of the energy cut in the presence of ISR. Entry values refer only to the real pair production cross section. Third picture: relative effect of ISR correction for exact matrix element and t-channel approximation.

In figure 8 the comparison between the exact matrix element and t-channel approximation is made in the presence of ISR with the CALO2 setup in the narrow-wide acceptance at LEP1/SLC energies and with the same notation previously used. An apex γ means that the relative correction is dressed by ISR.

As can been seen, the presence of ISR becomes more and more important in the soft region (small z values) up to modifying pair correction by a 25%, but it does not alter the analysis in tree level approximation discussed in the previous section.

8 Conclusions

The progress in the reduction of the sources of theoretical error to Bhabha cross section at small angle, driven by increased experimental accuracy, showed the need of reducing the uncertainty associated to the light pair contribution.

Till now the theoretical error to SABH scattering due to pair production is evaluated by using MC results based on t-channel approximation and with the aid of analytical means. In order to improve the present situation, a new MC program for $e^+e^- \to e^+e^-e^+e^-$ process was presented. It includes the exact QED four-fermion matrix element, ISR in the collinear approximation, and realistic selection criteria. The results obtained by means of that program were compared with the best approximations present in the literature, either analytical or numerical.

Two kinds of contribution form the theoretical error: the physical error, due to matrix element approximation, and the technical error, due to numerical integration. The comparison between the exact matrix element calculation performed in the present paper and the t-channel approximation adopted in the literature showed that the physical error committed by using such approximation at LEP1/SLC energies is within 30% with the exception of the hard region. Indeed in such region it grows up to 75% of the correction, while in the soft and intermediate region it can be much lower. Thus the calculation drawn with the t-channel approximation is within the physical error quoted in the literature [10] in the experimentally relevant kinematic region. At LEP2 energies the physical error due to the approximation is smaller and it is within 10%.

Concerning the present calculation, the physical error associated to electron pairs amounts in neglecting Z-boson contributions to the tree level matrix element, in approximating ISR by the collinear structure functions, and in omitting pair correction exponentiation as for instance done in ref. [10]. Relatively to the whole correction, the physical error due to these sources can be estimated within 5%, while the technical error amounts only to a few per cent, leading to a conservative 10% of the correction for the total theoretical error.

Further light pair production sums up the electron pair production with other contributions, e.g. muon pair production. Such effect amounts for muon pair production to a 10-20% of the electron contribution. However, since the present algorithm can compute also the effect of muon pairs, the total theoretical error can be estimated at 30% level of the whole correction, as due to approximations in electron and muon pair corrections and to neglecting heavier pair contributions.

A review for the contribution to the theoretical error at LEP1/SLC is shown in table 7. In the first column are listed the values of table 1 [3] and in the second column the updated values to the latest results for photonic

$O(\alpha^2 L)$ corrections [4, 7, 8], while in the third column the values are further updated to the result of the present analysis, when taking into account electron and muon pair corrections and a total error estimate of 30%.

Table 7: Theoretical error in SABH scattering at LEP1/SLC. The first column (see also table 1) refers to ref. [3], the second column takes into account the results of refs. [4, 7, 8], the third column updates to the present analysis.

Type of correction/error	ref. [3] (%)	ref. [4] (%)	updated (%)
missing photonic $O(\alpha^2 L)$	0.100	0.027	0.027
missing photonic $O(\alpha^3 L^3)$	0.015	0.015	0.015
vacuum polarization	0.040	0.040	0.040
light pairs	0.030	0.030	0.010
Z-exchange	0.015	0.015	0.015
total	0.110	0.061	0.054

Table 7 shows that the theoretical error for SABH scattering, because of the reduction of the pair production error, is now close to 0.05% and so comparable with the experimental accuracy. The conclusions, drawn for LEP1/SLC, can also be extended to LEP2 energies and lead to the reduction of the theoretical error shown in table 8.

Table 8: Theoretical error in SABH scattering at LEP2. The first column (see also table 1) refers to ref. [3], the second column takes into account the results of refs. [4, 7, 8], the third column updates to the present analysis.

Type of correction/error	ref. [3] (%)	ref. [4] (%)	updated (%)
missing photonic $O(\alpha^2 L)$	0.200	0.040	0.040
missing photonic $O(\alpha^3 L^3)$	0.030	0.030	0.030
vacuum polarization	0.100	0.100	0.100
light pairs	0.050	0.050	0.015
Z-exchange	0.000	0.000	0.000
total	0.250	0.122	0.113

It is worth noticing that now the major contribution to the theoretical

error is due to the hadronic uncertainty in the vacuum polarization correction. Thus, if the new determinations [9] of $\alpha_{\rm QED}(M_Z)$ could be drawn to the 1 GeV mass scale too, the total error could decrease further.

The present work was conceived to lower the theoretical error on SABH scattering due to light pair production. Yet, in order to manage the numerical and theoretical questions, techniques of a wider range of applicability were implemented. Chiefly, to deal with multiperipheral dynamics, Weizsäcker-Williams approximation played an important rôle as a guideline to develop a suited importance sampling and it led to a numerical recipe that can be further applied to perform phenomenological studies of processes involving particles lost in the beam pipe.

Therefore, future developments could deal with the evaluation of pair correction to two fermion production large angle processes at present and future e^+e^- colliders. Experimentally relevant processes are $e^+e^- \to e^+e^-$, whose interest is for luminosity measurements at DAΦNE and NLC, and $e^+e^- \to$ hadrons in the context of precision studies of the electroweak interaction at LEP and beyond.

Other fields of interest concern background processes for WW physics and searches for new physics, as very recently addressed in ref. [21] for the single W production case, and two photon collision processes.

All these studies will require the upgrade of the QED matrix elements considered in the present paper to the full electroweak ones. It is worth noticing that this generalization could be worked out quite directly by virtue of the automatic algorithm employed in the present approach.

Acknowledgements

M.Moretti was supported by a Marie Curie fellowship (TMR-ERBFMBICT 971934). A.Pallavicini wishes to thank INFN Sezione di Pavia for the support and for computer facilities.

References

[1] See for example G.Montagna, O.Nicrosini, F.Piccinini, *Riv.Nuovo Cimento* **21**, n.9 (1998) 1.

[2] G.M.Dallavalle, *Acta Phys.Pol.* **28** (1997) 901 and references therein;
B.Bloch, talk given at *XXIX International Conference on High Energy Physics*, Vancouver, July 23-29 1998.

[3] S.Jadach, O.Nicrosini et al., in *Physics at LEP2*, CERN **96-01** G.Altarelli, T.Sjöstrand and F.Zwirner eds., Vol.2 pg.229;
A.Arbuzov et al., *Phys.Lett.B* **389** (1996) 129.

[4] B.F.L.Ward, S.Jadach, M.Melles, S.A.Yost, `hep-ph/9811245`, talk given by B.F.L.Ward at *XXIX International Conference on High Energy Physics*, Vancouver, July 23-29 1998.

[5] S.Jadach, W.Placzek, B.F.L.Ward, *Phys.Lett.B* **353** (1995) 349;
S.Jadach, E.Richter Was, B.F.L.Ward, Z.Was, *Phys.Lett.B* **353** (1995) 362;
S.Jadach et al., *Comput.Phys.Comm.* **102** (1997) 229.

[6] S.Eidelman, F.Jegerlehner, *Z.Phys.C* **67** (1995) 585;
H.Burkhardt, B.Pietrzyk, *Phys.Lett.B*, **356** (1995) 398.

[7] G.Montagna, O.Nicrosini, F.Piccinini, *Phys.Lett.B* **385** (1996) 348. See also ref. [1].

[8] S.Jadach, M.Melles, B.F.L.Ward, S.A.Yost, *Phys.Lett.B* **377** (1996) 168, *Nucl.Phys.Proc.Suppl.* **51C** (1996) 164;
S.Jadach et al., in *Proceedings of the 28th International Conference on High Enrgy Physics*, Z.Ajduk and A.K.Wroblewski eds. (World Sientific, Singapore 1997), Vol.II,pg.1072;
B.F.L.Ward et al., *Acta Phys.Pol.B* **28** (1997) 925.

[9] R.Alemany, M.Davier, A.Höcker, *Eur.Phys.J.C2* (1998) 123;
M.Davier, A.Höcker, *Phys.Lett.B* **435** (1998) 427, `hep-ph/9805470`;
J.H.Kühn, M.Steinhauser, MPI-PHT-98, `hep-ph/9802241`;
S.Groote, J.G.Korner, K.Shilcher, N.F.Nasrallah, MZ-TH-98-02, `hep-ph/9802374`;
J.Erler, UPR-796T, `hep-ph/9803453`.

[10] S.Jadach, M.Skrzypek, B.F.L.Ward *Phys.Rev.D* **55** (1997) 1206.

[11] A.Arbuzov et al., *J.Exp.Theor.Phys.* **81** (1995) 638, *Nucl.Phys. Proc.Suppl.* **51C** (1996) 154, *Nucl.Phys.B* **485** (1997) 457, *Phys.Lett.B*

394 (1997) 218, *Phys.Lett.B* **399** (1997) 312;
N.P.Merenkov et al., *Acta Phys.Pol.B* **28** (1997) 491.

[12] S.Jadach, M.Skrzypek, B.F.L.Ward *Phys.Rev.D* **47** (1993) 3733.

[13] C.F.Weizsäcker, *Z.Phys.* **88** (1934) 612;
E.J.Williams, *Phys.Rev.* **45** (1934) 729.
See also S.Frixione, M.Mangano, P.Nason, G.Ridolfi, *Phys.Lett.B* **319** (1993) 339.

[14] V.N.Baier, V.S.Fadin, V.A.Khoze, E.A.Kuraev, *Phys.Rep.* **78** (1981) 293 and references therein.

[15] F.Caravaglios, M.Moretti, *Phys.Lett.B* **358** (1995) 332.

[16] F.A.Berends, P.H.Daverveldt, R.Kleiss, *Nucl.Phys.B* **253** (1985) 421, *Comput.Phys.Comm.* **40** (1986) 271,285,309;
P.Aurence, G.A.Schuler et al., in *Physics at LEP2*, CERN **96-01** G.Altarelli, T.Sjöstrand and F.Zwirner eds., Vol.1 pg.291;
L.Lönnblad, M.Seymour et al., *ibidem*, Vol.2 pg.187;
A.Courau, talk given at *VI EuroDAΦNE Collaboration Meeting*, Barcelona, November 7-9 1997.

[17] F.Boudjema, B.Mele et al., in *Physics at LEP2*, CERN **96-01** G.Altarelli, T.Sjöstrand and F.Zwirner eds., Vol.1 pg.207;
D.Bardin, R.Kleiss et al., *ibidem*, Vol.2 pg.3.

[18] M.Moretti, *Nucl.Phys.B* **484** (1996) 3;
F.Caravaglios, M.Moretti, *Z.Phys.C* **74** (1997) 291;
G.Montagna, M.Moretti, O.Nicrosini, F.Piccinini, *Eur.Phys.J.C* **2** (1998) 483;
G.Montagna, M.Moretti, O.Nicrosini, F.Piccinini, `FNT/T-98/07`, `CERN-TH/98-238`, `hep-ph/9807465`, to appear in *Nucl.Phys.B*;
F.Caravaglios, M.L.Mangano, M.Moretti, R.Pittau, `hep-ph/9807570`, `CERN-TH/98-249`, to appear in *Nucl.Phys.B*.

[19] R.Barbieri, J.A.Mignaco, E.Remiddi, *Nuovo Cimento* **11A** (1972) 824;
G.J.H.Burgers, *Phys.Lett.B* **164B** (1985) 167.

[20] E.A.Kuraev, V.Fadin, *Sov.J.Nucl.Phys.* **41** (1985) 466;
G.Altarelli, G.Martinelli, in *Physics at LEP2*, CERN **86-02** J.Ellis,

R.Peccei eds., Vol.1 pg.47;
O.Nicrosini, L.Trentadue, *Phys.Lett.B* **196** (1987) 551, *Z.Phys.C* **39** (1998) 479;
F.A.Berends, G.Burgers, W.L.van Neerven, *Nucl.Phys.B* **297** (1988) 429;
S.Jadach, M.Skrzypek, *Z.Phys.C* **49** (1991) 577;
M.Skrzypek, *Acta Phys.Pol.B* **23** (1992) 135;
M.Cacciari, A.Deandrea, G.Montagna, O.Nicrosini *Europhys.Lett.* **17** (1992) 123.

[21] G.Passarino, `hep-ph/9810416`.

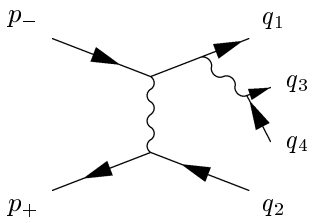
p_-
q_1
q_3
q_4
p_+
q_2

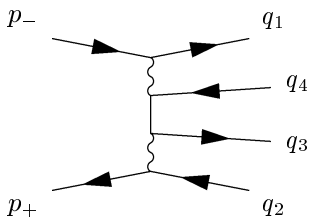
p_-
q_1
q_4
q_3
p_+
q_2

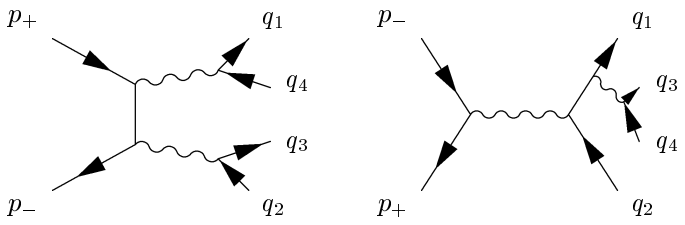
p_+
q_1
q_4
q_3
p_-
q_2
p_-
q_1
q_3
q_4
p_+
q_2

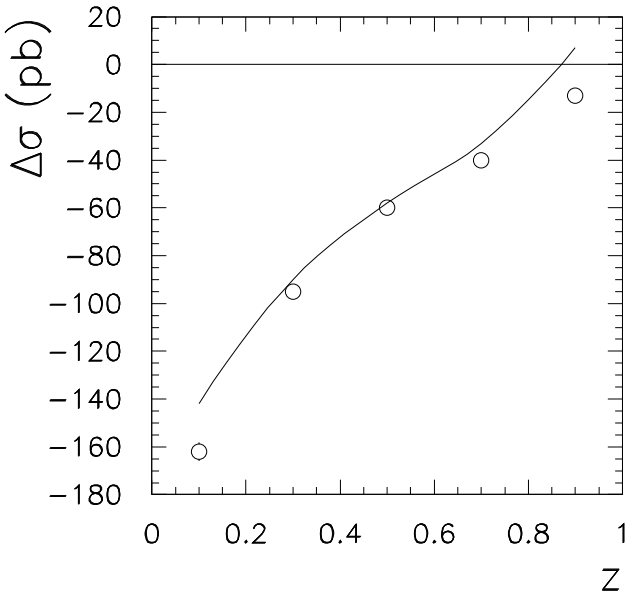
20
0
−20
−40
−60
−80
−100
−120
−140
−160
−180
Δσ (pb)
0
0.2
0.4
0.6
0.8
1
Z

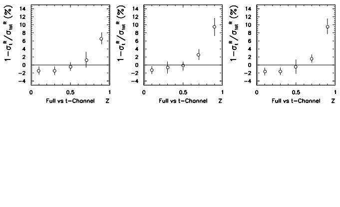

Δσ/σ0 *10^4
NN Calo2 Setup
NW Calo2 Setup
WW Calo2 Setup
Z
1−σt^R/σtot^R (%)
Full vs t−Channel